

## RESEARCH ARTICLE

# Biochemical, structural, and functional studies reveal that MAB\_4324c from *Mycobacterium abscessus* is an active tandem repeat *N*-acetyltransferase

Husam M. A. B. Alsarraf<sup>1,2</sup> , Kien Lam Ung<sup>1,†</sup> , Matt D. Johansen<sup>1,\*</sup> , Juliette Dimon<sup>1</sup>, Vincent Olieric<sup>3</sup> , Laurent Kremer<sup>1,4</sup>  and Mickaël Blaise<sup>1</sup> 

<sup>1</sup> IRIM, CNRS, Université de Montpellier, France

<sup>2</sup> Department of Molecular Biology and Genetics, Aarhus University, Aarhus, Denmark

<sup>3</sup> Swiss Light Source, Paul Scherrer Institute, Villigen, Switzerland

<sup>4</sup> INSERM, IRIM, Montpellier, France

## Correspondence

M. Blaise, IRIM, CNRS, Université de Montpellier, Montpellier, France  
 Tel: +33 (0)434359468  
 E-mail: mickael.blaise@irim.cnrs.fr

## Present address

\*Faculty of Science, Centre for Inflammation, School of Life Sciences, Centenary Institute and University of Technology Sydney, NSW, Australia  
<sup>†</sup>Department of molecular biology and Genetics, Aarhus University, Denmark

(Received 10 February 2022, revised 4 April 2022, accepted 7 April 2022, available online 3 June 2022)

doi:10.1002/1873-3468.14360

Edited by Dietmar Manstein

*Mycobacterium abscessus* is a pathogenic non-tuberculous mycobacterium that possesses an intrinsic drug resistance profile. Several *N*-acetyltransferases mediate drug resistance and/or participate in *M. abscessus* virulence. Mining the *M. abscessus* genome has revealed genes encoding additional *N*-acetyltransferases whose functions remain uncharacterized, among them MAB\_4324c. Here, we showed that the purified MAB\_4324c protein is a *N*-acetyltransferase able to acetylate small polyamine substrates. The crystal structure of MAB\_4324c was solved at high resolution in complex with its cofactor, revealing the presence of two GCN5-related *N*-acetyltransferase domains and a cryptic binding site for NADPH. Genetic studies demonstrate that MAB\_4324c is not essential for *in vitro* growth of *M. abscessus*; however, overexpression of the protein enhanced the uptake and survival of *M. abscessus* in THP-1 macrophages.

**Keywords:** GCN5; infection; intracellular survival; macrophage; *Mycobacterium abscessus*; *N*-acetyltransferase; X-ray structure

*Mycobacterium abscessus* (Mab) is an opportunistic non-tuberculous human pathogen [1]. The *Mycobacterium abscessus* complex encompasses three subspecies *M. abscessus sensu stricto*, *M. abscessus* subsp. *massetense*, and *M. abscessus* subsp. *bolletii*. Several epidemiological studies have emphasized a possible human–human transmission cycle of Mab [2,3] and demonstrated that only a few dominant clones are

circulating [4], which is in favor of global transmission of Mab in humans. The prevalence of Mab pulmonary infection was estimated to be below 1 per 100 000 inhabitants in the United States; however, this number might be underestimated and Mab infections are expected to be on the rise [5]. Patients with underlying genetic and structural abnormalities, such as those with bronchiectasis or CF, are particularly susceptible

## Abbreviations

ACO, acetyl-CoA; ADP, adenosine diphosphate; AMK, amikacin; APR, apramycin; CF, cystic fibrosis; CFU, colony-forming units; CoA, coenzyme A; DTNB, 5,5-dithio-bis-(nitrobenzoic acid); Eis, enhanced in intracellular survival; GNAT, GCN5-related *N*-acetyltransferase; HYG, hygromycin B; IPTG, isopropyl- $\beta$ -D-thiogalactoside; KAN, kanamycin; Mab, *Mycobacterium abscessus*; MmpL, mycobacterial membrane protein large; MmpS, mycobacterial membrane protein small; NADH, reduced nicotinamide adenine dinucleotide; NADPH, reduced nicotinamide adenine dinucleotide phosphate; OADC, oleic acid-albumin-dextrose-catalase; PEG, polyethylene glycol; SEC, size-exclusion chromatography; SPDN, spermidine; SPR, spermine; TEV, Tobacco Etch Virus; TYR, tyramine; WT, wild-type;  $\beta$ -ME,  $\beta$ -mercaptoethanol.

to Mab infection [1]. The prevalence of Mab infection among CF patients is estimated to range from 5% to 20% [6]. Treatments of Mab infections are particularly long and are often associated with therapeutic failures. The poor efficacy of drug treatments is correlated with the intrinsic resistance of Mab to most common antibiotics, including first-line anti-tubercular isoniazid and rifampicin [1,7]. In addition to the low permeability of the mycobacterial cell wall which limits the penetration of small molecules, Mab has developed multiple resistance mechanisms that include drug efflux activity mediated by MmpS/MmpL transporters [8,9], modifications or hydrolysis of the drug [7,10–15], and/or alteration of the drug target [16,17] ultimately incapacitating drug activity.

Mab is thought to be an environmental bacterium that colonizes different hosts and can persist within amoebae [18]. While Mab can replicate within amoebae, genomic analyses highlighted the accumulation of non-mycobacterial genes, which are thought to have been acquired to promote environmental persistence and nutrient acquisition. Furthermore, thorough transcriptomic analyses deciphered the differential gene expression pattern in correlation with the lifestyle of Mab and identified several genes which were shown to be upregulated when Mab is inside amoebae or in murine macrophages, thus highlighting the occurrence of an adaptive transcriptional program in response to various stresses encountered within the cell [19]. To this end, the *MAB\_4532c* gene, encoding the Eis2 protein, plays a critical role in the intramacrophage survival of Mab [19]. Eis proteins that belong to the GCN5-related *N*-acetyltransferase (GNAT) family indeed play a key role in the intracellular survival of other pathogenic mycobacteria and notably *Mycobacterium tuberculosis* [20,21]. In addition, due to their *N*-acetyltransferase activity, Eis proteins can modify aminoglycoside antibiotics through acetylation, thereby impairing their binding to the ribosomes and leading to drug resistance [22,23]. Moreover, Eis2 confers high-level resistance to aminoglycosides in Mab [12–14]. A very close homologue of Eis2, named Eis1, is neither required for intracellular survival [19] nor aminoglycoside resistance, suggesting that it possesses another function that remains to be defined [12,14]. Together, these findings exemplify the need to experimentally address the substrate specificity and biological function of GNAT proteins despite their high homology levels with well-described homologues.

Transcriptomic approaches have been largely employed to identify key players of the drug resistance and/or virulence response in mycobacteria. As such, gene regulation studies have revealed that *MAB\_4324c*

is more highly expressed under intracellular growth conditions as compared to planktonic cultures [19]. In contrast, *MAB\_4324c* expression is downregulated in a Mab *whiB7* deletion mutant [15]. *WhiB7* represents a master transcription regulator controlling gene expression involved in the stress response and confers resistance to several classes of antibiotics, opening up the possibility that *MAB\_4324c* might participate in these processes. Furthermore, RNAseq analyses identified several genes including *MAB\_4324c* that were upregulated upon exposure of Mab to clinically relevant antibiotics, such as amikacin, clarithromycin, and tigecycline [24].

Considering the importance of GNAT enzymes in mycobacterial drug resistance mechanisms and virulence, and because *MAB\_4324c* encodes a predicted GNAT, this study was undertaken to functionally characterize the role of *MAB\_4324c* in Mab. Herein, a combination of biochemical and structural approaches was used to demonstrate that *MAB\_4324c* is an active tandem repeat *N*-acetyltransferase. Genetic studies showed that while *MAB\_4324c* is dispensable for planktonic growth, its overexpression confers an intracellular growth advantage to Mab in THP-1 macrophages.

## Materials and methods

### MAB\_4324c cloning into the expression plasmid

The *MAB\_4324c* gene was synthesized by Genscript with codon-optimized for *Escherichia coli* expression and cloned into the expression vector pET30a. The sequences encoding for the hexahistidine- and S-tags followed by the TEV protease site were included in the 5'-end of the gene.

### MAB\_4324c expression and purification

The pET30a::*MAB\_4324c* construct was transformed into *E. coli* BL21 (DE3) resistant to Phage T1 (New England Biolabs, Evry, France) harboring plasmid encoding rare tRNAs. An overnight pre-culture was used to inoculate a 12 L culture of Luria broth (LB) media supplemented with 50 and 30  $\mu\text{g}\cdot\text{mL}^{-1}$  of KAN and chloramphenicol. The culture was grown until the exponential growth phase was reached and subjected to cold shock in an ice bath before induction of the protein expression with 1 mM of IPTG (Euromedex, Souffelweyersheim, France) overnight at 18 °C. The bacteria were homogenized in lysis buffer A (50 mM Tris/HCl pH 8, 0.4 M NaCl, 20 mM imidazole, 1 mM benzamidinium and 5 mM  $\beta$ -ME). Bacteria were disrupted by sonication and centrifugated at 28 000 g. The soluble fraction was loaded onto a Ni-NTA Sepharose resin (Cytiva, Europe, GMBH) by gravity. The column was washed with buffer A and buffer B (50 mM Tris/HCl pH 8, 1 M NaCl and 5 mM  $\beta$ -ME). Proteins were eluted with

buffer C (50 mM Tris/HCl pH 8, 0.2 M NaCl, 5 mM  $\beta$ -ME and 400 mM imidazole). The eluate was dialyzed overnight at 4 °C in dialysis buffer D (50 mM Tris/HCl pH 8, 0.2 M NaCl and 5 mM  $\beta$ -ME) in the presence of His-tagged TEV protease in a 50 : 1 w/w ratio to remove the tags. The TEV protease and the uncleaved MAB\_4324c were separated from the untagged proteins by the passage of the dialyzed eluate through a Ni-NTA sepharose column. MAB\_4324c was collected in the flow-through and concentrated by ultra-filtration (centricon 10 kDa CW-Sartorius). Finally, MAB\_4324c was concentrated to 5 mg·mL<sup>-1</sup> and loaded onto a size-exclusion chromatography (SEC) column (Superdex 200 Increase 10/300 column from GE Cytiva) and eluted with buffer E (20 mM Tris/HCl pH 7.4 and 0.2 M NaCl).

### Determination of MAB\_4324c oligomeric by size-exclusion chromatography

The Superdex 200 Increase 10/300 GL column (Cytiva) was calibrated with the Gel Filtration Markers Kit for protein molecular weight (MW) ranging from 12 400 to 200 000 Da (Sigma-Aldrich, Saint-Quentin Fallavier, France). The MW markers and MAB\_4324c were eluted with buffer E as described above and at a flow rate of 0.4 mL·min<sup>-1</sup> at 8 °C. The partition coefficient ( $K_{av}$ ) of each protein was calculated with the following formula  $K_{av} = (V_e - V_0)/(V_t - V_0)$ , where  $V_e$  is the volume of elution of the proteins,  $V_t$  the volume of the column (24 mL), and  $V_0$  the void volume corresponding to the elution volume of dextran blue. The MW of MAB\_4324c was extrapolated from the semi-logarithmic plot of the partition coefficients,  $K_{av}$ , of the standard proteins marker versus their respective molecular masses on a logarithmic scale.

### Crystallization

MAB\_4324c crystals were grown in sitting drops using the MR Crystallization Plates™ (Hampton Research, Aliso Viejo, CA, USA) at 18 °C by mixing 1  $\mu$ L of 12 mg·mL<sup>-1</sup> protein supplemented with 2 mM acetyl-CoA (incubated for 1 h on ice), with 1  $\mu$ L of reservoir solution (2 M ammonium sulfate, 0.1 M HEPES pH 7.5 and 2% w/v PEG400). Cryoprotection was not employed before crystals were cryo-cooled in liquid nitrogen, as all cryoprotective conditions tested led to crystal damage. Consequently, ice rings were present on diffraction data but did not affect data processing or structure refinement.

### Data collection, structure determination, and refinement

X-ray data collection was performed at the X06DA-PXIII beamline at the Swiss Light Source (Table 2). A 360° native data set was collected at a wavelength of 1-Å with an oscillation of 0.2° and an exposure time of 0.1 s on PILATUS

2M-F detector [25]. A single-wavelength anomalous diffraction experiment from intrinsic sulfur atoms (S-SAD) consisting of 12  $\times$  360°  $\omega$  scans at varying values of  $\chi$  and  $\phi$  of the PRIGo multi-axis goniometer [26] was collected on a single crystal at 100 K at 2.075-Å wavelength using 0.2° oscillation 0.1 s exposure as previously described [27]. Data processing, scaling, and merging were performed using *XDS* and *XSCALE* [28]. The high-resolution data cutoff was based on the statistical indicators  $CC_{1/2}$  [29]. Substructure determination and phasing were performed with *SHELX* [30,31] using the *CRANK2* program [32]. The automatically built model using *CRANK2* was rebuilt with *Coot* [33] and refined with *Phenix* [34] against the native data set (Table 2). The structure factors and atomic coordinates were deposited at the Protein Data Bank under the accession entry 7Q3A.

### Kinetics assay

MAB\_4324c was concentrated to 7.5 mg·mL<sup>-1</sup> in buffer E supplemented with 50% glycerol for use in kinetic assays. The reaction was performed at 25 °C in a quartz cuvette and consisted of monitoring the production of 2-thio-5-nitrobenzoic acid (TNB; extinction coefficient of 14150 M<sup>-1</sup>·cm<sup>-1</sup> at 412 nm) resulting in the reduction of DTNB by the free CoA. Data points were recorded with a time interval of 5 s for 50–60 s using a Nanodrop2000c spectrophotometer (ThermoFisher Scientific, Villebon sur Yvette, France). All compounds and the enzyme were dissolved and diluted in buffer E. MAB\_4324c (0.25  $\mu$ M) was added to the reaction mixture consisting of DTNB (0.5 mM), ACO (0.5 mM) as well as substrates when requested in a final volume of 100  $\mu$ L. A reaction mixture lacking the substrate was used to determine the reaction background and to normalize the values. Standard errors were calculated from triplicates, and a nonlinear least-squares regression algorithm was used to determine the Michaelis–Menten equation (GRAPHPAD PRISM software, San Diego, CA, USA).

### Generation of an unmarked MAB\_4324c knockout mutant in *M. abscessus*

The  $\Delta$ MAB\_4324c *M. abscessus* strain was generated by the unmarked deletion strategy involving two recombination steps as described previously [35]. The MAB\_4324c (1059 bp) flanking regions (each around 1500 bp) were PCR-amplified using the Phusion polymerase (ThermoFisher Scientific) and the following primers (upstream region FW: 5'-CCGGCTAGCTTCGTCAACAAGAAACTCATCCGCACCCTGTGAGCCAG-3', upstream region RV: 5'-GTCGCAAATAGGGTTGAACCCATGACATCCCACACGCAATTGGTGAACCGTTTCGATCAGCCTGATCAAACAGTTC-3', downstream region FW: 5'-GAACT

GTTTGATCAGGCTGATCGAACGGTTCACCAATTGCG TGTGGGATGTCATGGGTTCAACCCATTTGCGAC-3', downstream region RV: 5'-ACCGTTAACGCTGACGGG CGGGTTCAGAGTGAAGGT-3'). Amplicons were purified and treated with restriction enzymes (all from NewEngland Biolabs), ligated into pUX1-*katG<sub>Mtb</sub>*, and digested with *NheI* and *HpaI* restriction sites, where the flanking regions were ligated at the *MfeI* restriction site.

The resulting plasmid was transformed into electro-competent Mab CIP104536<sup>T</sup>, smooth variant [18]. Transformed bacteria were placed at 37 °C for 3 h under agitation before plating on Middlebrook 7H10 (Sigma-Aldrich) supplemented with oleic acid-albumin-dextrose-catalase (OADC) enrichment (7H10<sup>OADC</sup>) and 250 µg·mL<sup>-1</sup> KAN. The selection of colonies was based on resistance to KAN and tdTomato expression (red fluorescent colonies) as an indicator for the first recombination event. Selected red colonies were grown after 4 days in Middlebrook 7H9 broth (Sigma-Aldrich) supplemented with OADC, 0.025% tyloxapol and 250 µg·mL<sup>-1</sup> KAN. Bacteria were pelleted, washed thrice, and resuspended in an antibiotic-free medium. Cultures were then incubated overnight at 37 °C under agitation to allow for the second recombination event to occur. Bacteria were then plated on 7H10<sup>OADC</sup> plates supplemented with 50 µg·mL<sup>-1</sup> isoniazid (INH) and incubated at 37 °C for 4 days. INH-resistant and non-fluorescent colonies were genotyped by PCR to identify the mutants. Proper gene deletion was subsequently confirmed by PCR and sequencing.

### Overexpression of MAB\_4324c in *M. abscessus*

MAB\_4324c was amplified by PCR from genomic DNA using the following primers, Fw: 5'-AACGAATTC ATGACATCCACACGGTACCGACGGC-3', Rv: 5' CGC GTTAACCTCACTTCTCGAACTGCGGGTGGCTCCAGA ACTGTTTGATCAGGCTGATCGAACGGTT-3', (restriction sites are underlined) and cloned into the episomal pMV261 [36] and into the integrative pMV306, both cut with *EcoRI* and *HpaI*. This cloning strategy allows gene expression under the control of the strong *hsp60* promoter and enabled the addition of a strep tag at the C terminus of MAB\_4324c. The pMV261::MAB\_4324c and pMV306::MAB\_4324c constructs were introduced into electro-competent Mab WT and  $\Delta$ MAB\_4324c strains. The transformed bacteria were plated on 7H10<sup>OADC</sup> agar containing 250 µg·mL<sup>-1</sup> KAN. Individual colonies were then grown in 10 mL of Middlebrook 7H9<sup>OADC</sup> supplemented with 0.025% tyloxapol and 250 µg·mL<sup>-1</sup> KAN at 37 °C for 4 days, harvested, and frozen at -80 °C.

### Assessment of protein expression by western blotting

Bacteria were disrupted by bead-beating and sonication and centrifuged at 20 000 g, at 4 °C. The total proteins from the crude extract (about 100 µg) were separated by

SDS/PAGE and were then blotted onto a nitrocellulose membrane (Cytiva) in transfer buffer [20 mM Tris, 150 mM glycine and 10–20% (v/v) ethanol]. The membrane was treated with blocking buffer: PBS 1X, 5% (w/v) skimmed milk and 0.2% (v/v) Tween 20. Membranes were first incubated either with a primary anti-Strep-tag monoclonal antibody (dilution 1/10 000; Sigma-Aldrich) or with a rabbit anti-acetyl lysine primary antibody (dilution 1/500–1/1000; abcam21623) and subsequently incubated with a secondary anti-mouse monoclonal antibody or an anti-rabbit antibody conjugated to the horseradish peroxidase (dilution 1/2000–1/5000; Sigma-Aldrich). Immunoreactive bands were revealed using the luminol-based reaction (SuperSignal<sup>TM</sup>—Thermo Fisher Scientific) and imaged using a Chemidoc (Bio-Rad, Marnes la Coquette, France).

### Macrophage infection with *M. abscessus* strains

THP-1 macrophages were grown at 37 °C in a 5% CO<sub>2</sub> incubator in RPMI 1640 supplemented with 10% FBS (RPMI<sup>FBS</sup>) and differentiated for 48 h with 20 ng·mL<sup>-1</sup> phorbol myristate acetate (PMA). Exponentially growing Mab strains were harvested and resuspended in PBS 1X. Single-cell bacteria were produced by passage through a 26.5-gauge needle (20 times) and then further filtered through a 5.0 µm filter (Merck Millipore, Saint-Quentin en Yvelines, France). THP-1 cells were infected at a 2 : 1 (bacteria : macrophage) Multiplicity of Infection (M.O.I.) and grown at 37 °C in the presence of 5% CO<sub>2</sub>. After 4 h incubation, cells were washed thrice with PBS 1X and incubated with RPMI<sup>FBS</sup> supplemented with 250 µg·mL<sup>-1</sup> AMK for 2 h to eliminate extracellular bacilli. Infected THP-1 macrophages were cultured in RPMI<sup>FBS</sup> supplemented with AMK maintained at 50 µg·mL<sup>-1</sup>. Bacterial extracellular growth was prevented by refreshing the culture medium containing AMK 50 µg·mL<sup>-1</sup> every two days. Before plating the bacteria, THP-1 macrophages were washed thrice with PBS 1X. Cell lysis was achieved with 100 µL of 1% Triton X100 in PBS 1X. Then, 900 µL of PBS 1X was added to each well and tenfold dilutions were plated onto LB agar. This procedure was repeated at 0, 1, 3, and 5 days post-infection. After 5 days of incubation at 37 °C, the number of CFU was assessed. The CFUs counts were plotted on a logarithmic scale, and the standard error bars were calculated using the GRAPH PAD PRISM software.

### Growth curves of *M. abscessus* strains

Cultures of 20 mL were inoculated with single-cell preparations in 7H9<sup>OADC</sup> supplemented with 0.025% tyloxapol (starting OD<sub>600 nm</sub> of 0.05) and incubated at 37 °C under agitation (100 rpm) for 5 days. The OD was monitored daily and the values were plotted, and error bars were calculated using the GRAPH PAD PRISM software.



## Drug susceptibility testing

The minimal inhibitory concentration (MIC) experiments were determined for the following antibiotics: bedaquiline, cefoxitin, ethambutol, vancomycin, ciprofloxacin, imipenem, kanamycin B, hygromycin B, amikacin, tigecycline, and clofazimine. MICs were determined according to the Clinical and Laboratory Standards Institute (CLSI) guidelines [37]. The broth microdilution method was used in cation-adjusted Mueller–Hinton broth (CaMHB) with single-cell preparations of Mab wild-type,  $\Delta$ MAB\_4324c and corresponding to  $5 \times 10^6$  CFU·mL<sup>-1</sup>. Serial dilutions of the drug (100  $\mu$ L) were added to 100  $\mu$ L of bacterial suspension and incubated for 3–5 days at 30 °C.

## Results and Discussion

### MAB\_4324c is an active *N*-acetyltransferase

Sequence analysis of MAB\_4324c using the Pfam server [38] predicted the presence of a well-conserved GNAT domain in its C terminus as well as a second GNAT domain displaying lower conservation in its N terminus. This analysis indicates that MAB\_4324c may belong to the tandem repeat *N*-acetyltransferase family. MAB\_4324c shares a low-protein sequence identity with the well-characterized Eis proteins and does not possess the same modular organization.

To inquire whether MAB\_4324c possesses *N*-acetyltransferase activity, we performed a biochemical analysis of the protein. First, MAB\_4324c was recombinantly expressed in *E. coli* and the soluble protein was subsequently purified following a three-step purification procedure. Highly pure MAB\_4324c preparations were obtained (Fig. 1A) and assessed for molecular weight determination by size-exclusion chromatography (SEC) (Fig. 1A). The protein was eluted at a volume of 14.5 mL using a Superdex 200 10/300 GL Increase column. This elution profile corresponds to an apparent molecular weight of 42.6 kDa, which is in line with the theoretical mass of 39.1 kDa. This indicates that the protein is a monomer in solution.

We next assessed the activity of MAB\_4324c with a few substrates known as substrates of *N*-acetyltransferases belonging to different classes [39,40]. *N*-acetyltransferases substrates are highly diverse and, without any closely related protein whose function is known it was difficult to determine the substrate of MAB\_4324c. As the Eis members of the GNAT protein in mycobacteria can modify aminoglycosides through acetylation of their primary amines, we first tested if MAB\_4324c could modify this class

of antibiotics. The near absence of or very low activity could be noticed using APR, HYG, or AMK as substrates and ACO as a cofactor (Fig. 1B). We next tested substrates suited for numerous GNAT and all possessing primary amines notably histamine, tyramine, spermine, and spermidine (Fig. 1B) [14,40]. This screening identified only spermine and spermidine as substrates of MAB\_4324c, with a slightly better apparent activity for spermidine (Fig. 1B). To ensure that the reaction we observed was enzyme-specific, additional control experiments were performed with the heat-inactivated enzyme or with reactions lacking either the enzyme or the cofactor. As expected, the *N*-acetyltransferase activity was only detected in the presence of a functional MAB\_4324c (Fig. S1A). The kinetic parameters of MAB\_4324c for spermidine and acetyl-CoA were determined (Table 1) (Fig. 1C,D and Fig. S1B,C). The relatively low catalytic efficiency and very low  $K_M$  suggest that spermidine is not the cognate substrate of MAB\_4324c though these kinetic data attest that MAB\_4324c is an active *N*-acetyltransferase capable of transferring acetyl group to primary amines.

### MAB\_4324c is a tandem repeat *N*-acetyltransferase

To support the biochemical data, we engaged in structural studies of MAB\_4324c. We succeeded in obtaining exploitable crystals of the protein when it was co-crystallized with acetyl-CoA. Structure phasing was achieved through the sulfur-single-wavelength anomalous dispersion method (Table 2). The partial model built thanks to the anomalous map was further used to solve the structure obtained from a 2 Å resolution native dataset.

Two monomers occupy the asymmetric unit (Fig. 2A). Most of the residues could be rebuilt for the two monomers except for the first 11 and 12 residues of our expressed construct (that contains one extra Gly residue coming from the TEV cleavage site on top of the MAB\_4324c sequence) in monomers A and B, respectively. We could not build some residues of the loop between strands 8 and 9 due to very poor electron density in this area.

Crystal packing analysis did not argue in favor of a functional dimer and in agreement with the oligomeric state of the protein observed by SEC (Fig. 1A).

The MAB\_4324c overall structure (Fig. 2B) is composed of 12  $\beta$ -strands and 11  $\alpha$ -helices forming two GNAT domains interconnected to each other with two  $\beta$ -strands ( $\beta_6$  and  $\beta_{12}$ ). The structure can be divided

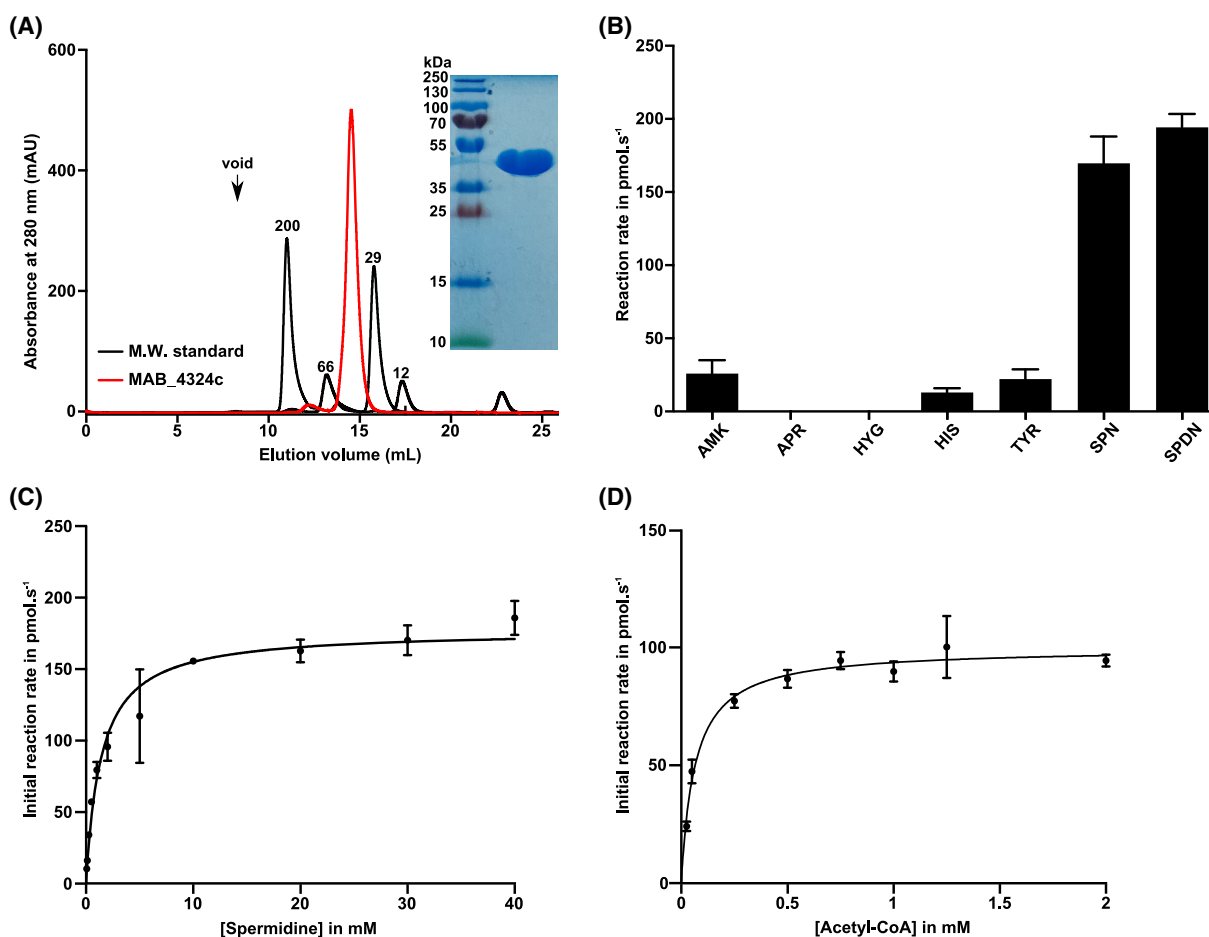


**Fig. 1.** Biochemical characterization of MAB\_4324c. (A) Coomassie Blue-stained SDS polyacrylamide gel electrophoresis attesting the purity of MAB\_4324c obtained after three steps of purification (10  $\mu$ g of protein were loaded on the gel). Estimation of the oligomeric state of MAB\_4324c, depleted from its tags, by SEC. The elution profile of the proteins used for calibration on the Superdex 200 increase 10/300 GL column is displayed as a black line, and the elution profile of MAB\_4324c is indicated in red. Calibration was established using  $\beta$ -amylase (200 kDa), bovine serum albumin (66 kDa), carbonic anhydrase (29 kDa), and cytochrome C (12.4 kDa), eluted with estimated volumes of 11.07, 13.2, 15.8, and 17.3 mL, respectively. The void volume indicated by the black arrow was estimated at 8.3 mL with dextran blue. The MAB\_4324c elution peak at 14.5 mL corresponds to an apparent molecular weight of 42.6 kDa. (B) Substrate specificity assessment of MAB\_4324c. The initial rates were determined in the presence of 10 mM of each of the following substrates: AMK, apramycin (APR), hygromycin B (HYG), histamine (HIS), tyramine (TYR), spermine (SPR), or spermidine (SPDN). Acetyl-CoA at 0.5 mM was used as a cofactor. (C) Michaelis-Menten curve used to determine the kinetic constants for spermidine in the presence of 0.5 mM of acetyl-CoA. (D) Michaelis-Menten curve was used to determine the kinetic constants for acetyl-CoA in the presence of 40 mM spermidine.

into two major subdomains: domain 1 in the N terminus is containing residues 1–177 ( $\alpha$ 1– $\alpha$ 6 and  $\beta$ 1– $\beta$ 6) and is a GNAT domain although the *e*-value ( $8.4 \times 10^{-5}$ ) for this signature motif is quite low when analyzed at the Pfam server. Domain 2 in the C terminus encompasses residues 178–352 ( $\alpha$ 7– $\alpha$ 11 and  $\beta$ 7– $\beta$ 12) and matches a GNAT domain signature with a much better score (*e*-value =  $3.9 \times 10^{-11}$ ) than domain 1. These two domains share 13% sequence identity and their superposition based on their secondary structure and over the main chain of 137

residues led to a r.m.s.d. value of 2.1 Å (not shown), attesting to a certain degree of structural divergence but not as high as it would have been expected based on the sequence homology.

The two monomers from the asymmetric unit are not equivalent in terms of ligand binding (Fig. 2A). The two C-terminal subdomains bind acetyl-CoA (Figs 2A and 3A). This ligand is in fact in two forms as an acetyl-CoA and as another one where acetyl-CoA is cleaved into CoA and acetate. All ligand occupancies were estimated to be 0.5 (Fig. S2).

**Table 1.** Kinetic parameters of MAB\_4324c.

Substrates	$V_{\max}$ (pmol.s <sup>-1</sup> )	$K_M$ (μM)	$k_{\text{cat}}$ (s <sup>-1</sup> )	$K_M/k_{\text{cat}}$ (m <sup>-1</sup> .s <sup>-1</sup> )
Acetyl-CoA	99.6 ± 0.02	63 ± 0.07	$0.39 \times 10^{-3} \pm 0.008$	0.16
Spermidine	186.4 ± 5	$1.66 \times 10^3 \pm 0.22$	$0.74 \times 10^{-3} \pm 3.8 \times 10^{-5}$	2.24

**Table 2.** X-ray data collection and refinement statistics. Values between parentheses are for the last resolution shell.

	MAB_4324c native	MAB_4324c Sulfur SAD
Wavelength (Å)	1	2.08
Resolution range (Å)	49.09–2.0 (2.072–2.0)	49.26–2.33 (2.39–2.33)
Space group	<i>P</i> 65 2 2	<i>P</i> 65 2 2
Unit cell (Å, °)	149.96 149.96 183.38, 90 90 120	150.49 150.49 184.14, 90 90 120
Total reflections	3 143 788 (302 942)	19 074 956 (230 331)
Unique reflections	82 207 (8058)	99 388 (7401)
Multiplicity	38.2 (37.6)	191.9 (31.1)
Completeness (%)	96.84 (99.98)	99.00 (99.30)
Mean <i>I</i> /σ( <i>I</i> )	39.58 (5.79)	32.18 (0.82)
Wilson <i>B</i> -factor (Å <sup>2</sup> )	26.2	48.55
<i>R</i> -meas	0.115 (0.87)	0.278 (4.43)
CC1/2	1 (0.95)	1 (0.45)
Reflections used in refinement	79 620 (8058)	
Reflections used for <i>R</i> -free	1969 (199)	
<i>R</i> -work	0.186 (0.183)	
<i>R</i> -free	0.225 (0.236)	
Number of non-hydrogen atoms	6620	
Macromolecules	5437	
Ligands	340	
Solvent	860	
Protein residues	679	
RMS (bonds, Å)	0.01	
RMS (angles, °)	1	
Ramachandran favored (%)	98.66	
Ramachandran allowed (%)	1.34	
Ramachandran outliers (%)	0	
Rotamer outliers (%)	0.36	
Clash score	3.6	
Average <i>B</i> -factor (Å <sup>2</sup> )	31.5	
Macromolecules	29.9	
Ligands	37.9	
Solvent	39.3	
PDB accession	7Q3A	

Unexpectedly, a ligand neither corresponding to acetyl-CoA nor CoA was bound to domain 1 in each of the two monomers of the asymmetric unit. The

clear simulated-annealed omit maps [41] allowed without ambiguity the identification of NADH in one monomer and NADPH in the second one (Fig. 3B). In one monomer of the asymmetric unit, NADH could be placed; however, in the other monomer, NADPH was modeled. Since none of these ligands were added exogenously during the crystallization process, it appears obvious that they were co-purified during the purification of MAB\_4324c. Of note, NADPH was not modeled in both chains as the phosphate group cannot pack due to steric hindrance with the symmetry mate (not shown) in chain B and electron density does not support the presence of the additional phosphate group (Fig. 3B).

To ensure that NADH and NADPH are the bound forms rather than their oxidized forms and to assess to which extent MAB\_4324c is bound to nicotinamide after purification, we performed a UV spectrum of the concentrated protein. In addition to the protein absorption peak at 280 nm, a second peak was detected at 340 nm and corresponding to NADH/NADPH (Fig. S3). The concentration of the NADH/NADPH in the sample was estimated to 70 μM, which corresponds to the MAB\_4324c concentration, indicating that the protein is saturated with the reduced forms of the nicotinamide groups since the oxidized NAD<sup>+</sup>/NADP<sup>+</sup> forms do not display absorption peak at 340 nm.

Acetyl-CoA (ACO) is recognized by twelve residues (Fig. 3A and Fig. 4), of which the side chain of H222 establishes a H-bond *via* one water molecule with the S atom of ACO. The sulfur is also contacted by the Y334 side chain. H222 and Y334 interact with the ACO S-group and thus are very likely to be important catalytic residues. This is particularly true for Y334 as it was already proposed that the side chain of the catalytic Y residue of the RimI acetyltransferase might be important as a general acid for the protonation of the ACO sulfhydryl group before the transfer of the acetyl group [42,43]. F219 interacts by hydrophobic interaction with the acetyl moiety that is also stabilized by the main chain of L287. The main chains of T328 and V289 form a H-bond with the NH and CO groups of the pantothenate. The phosphates of ADP are interacting with the main chains of W293 (*via* one water molecule), G295, Q300, and

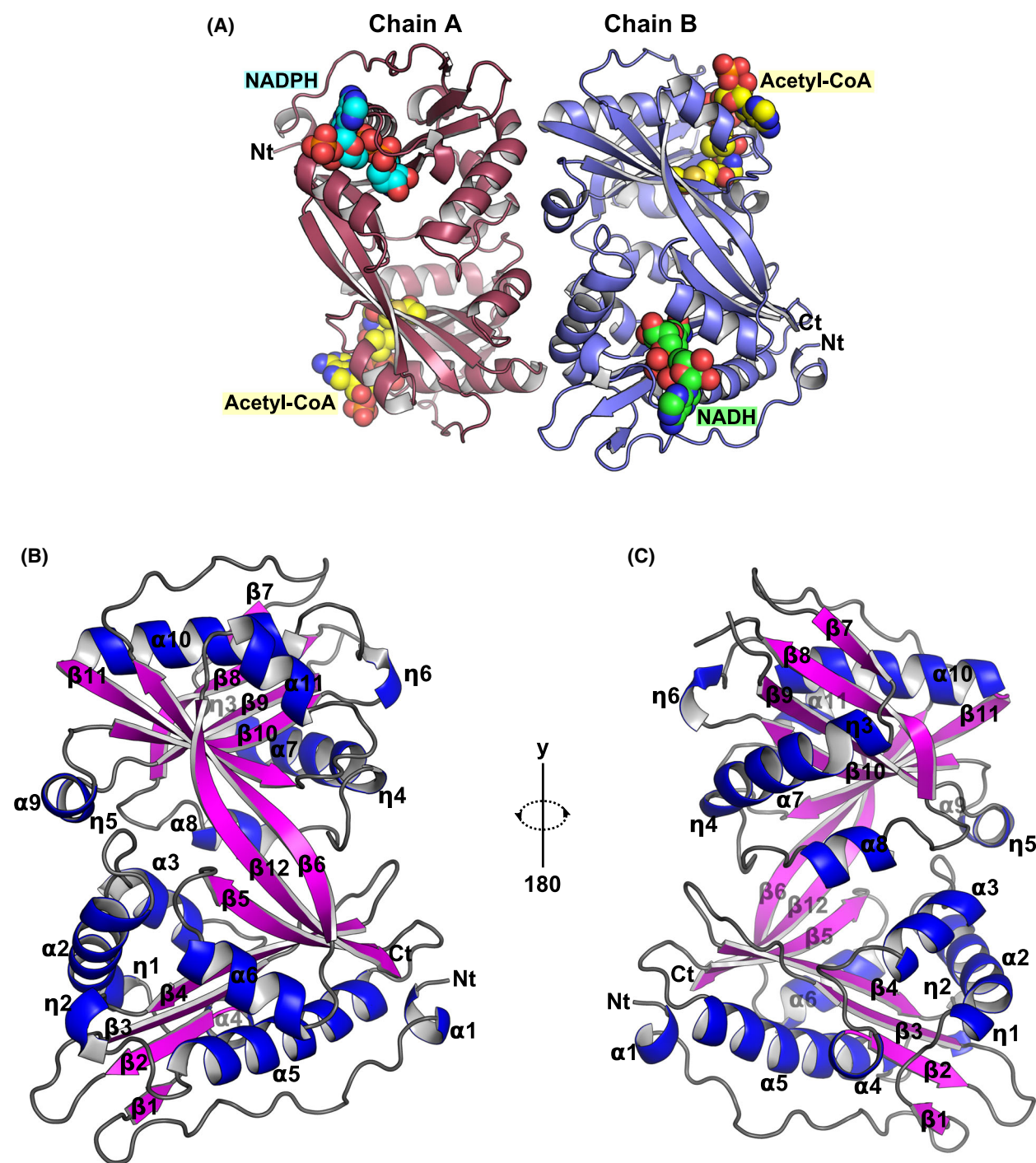


**Fig. 2.** Overall crystal structure of MAB\_4324c. (A) Composition of the asymmetric unit (A.U.). Two non-equivalent monomers of MAB\_4324c occupy the A.U. The two monomers are similar with the exception that the N-terminal subdomain of chain A binds NADPH while NADH is present in the N-terminal subdomain of chain B. Nt and Ct stand for N terminus and C terminus, respectively. (B) Overall structure of MAB\_4324c. Alpha ( $\alpha$ ) and  $3_{10}$  ( $\eta$ ) helices appear as blue cartoons, while beta-strands ( $\beta$ ) are colored in pink. Loops or coils are in gray.

K297, while the latter also binds the phosphate of the ACO ribose with its side chain. Finally, the side chain of R294 stacks the ACO.

Recognition of NADPH involves a complex network of interactions (Figs 3B and 4). The nicotinamide group of NADPH is contacted by the side



chains of Q133 and S154 as well as by the main chain of G114. F167, V129, and L166 mediate van der Waals interactions with the nicotinamide group. The hydroxyl of the ribose is contacted *via* H-bonds by the side chains of R121, T163 and the main chain of V116. The main chain of G122, E123, G124, and G126 tightly bind to the phosphate group of ADP moiety. The last interaction involves the side chain of R169 that establishes a H-bond with the ribose of the ADP.

The identification of a binding site for nicotinamide is particularly intriguing since, to our knowledge, GNAT domains have never been reported to bind to NADH/NADPH. It is well documented, however, that the type III GNAT enzymes are allosterically regulated by metabolic compounds [44]. This is the case for the GNAT enzyme (Rv0998) from *M. tuberculosis* which is allosterically regulated by cyclic AMP (cAMP) [45]. Activation of the enzyme's activity occurs upon binding of cAMP that triggers a large conformational switch. However, the GNAT domain is not the domain that binds cAMP [46]. The *N*-acetyltransferase MxKat from *Myxococcus xanthus* can bind to NADP<sup>+</sup> thanks to its N-terminal domain consisting of a Rossmann fold and binding to NADP<sup>+</sup> inhibits the enzyme activity [47]. To assess whether NADH or NADPH could play a role in regulating or modulating the enzymatic activity of MAB\_4324c, we compared the kinetic constants of MAB\_4324c for spermidine and in the presence of 0.1 mM of the reduced nicotinamide forms. The enzymatic properties were, however, not significantly affected by the addition of NADH or NADPH (Fig. S4 and Table S1). Interestingly, it was also proposed that the *N*-terminal GNAT domain of the mycothiol synthase is not catalytically active but its capacity to bind CoA may assist the enzyme to fold [48], suggesting that NADH or NADPH may be helpful for the folding of MAB\_4324c.

We then attempted to search for MAB\_4324c structural homologues whose biological function or enzymatic function was elucidated. This led to the identification of only two related structures (Fig. 4): the mycothiol synthase from *M. tuberculosis* (PDB id: 2C27) [48] bound to des-acetylmicothiol and CoA that possesses a r.m.s.d. of 1.9 Å and sequence identity of 19%, and the structure of glucosamine *N*-acetyltransferase bound to chitosan, GlmA, from *Clostridium acetobutylicum* (PDB id: 5KGP) sharing a r.m.s.d. of 2.6 Å and sequence identity of 12% [49]. These two enzymes are also tandem repeat *N*-acetyltransferases but are involved in different pathways. MshD is an essential enzyme for mycobacteria as it catalyzes the last step of mycothiol synthesis, a

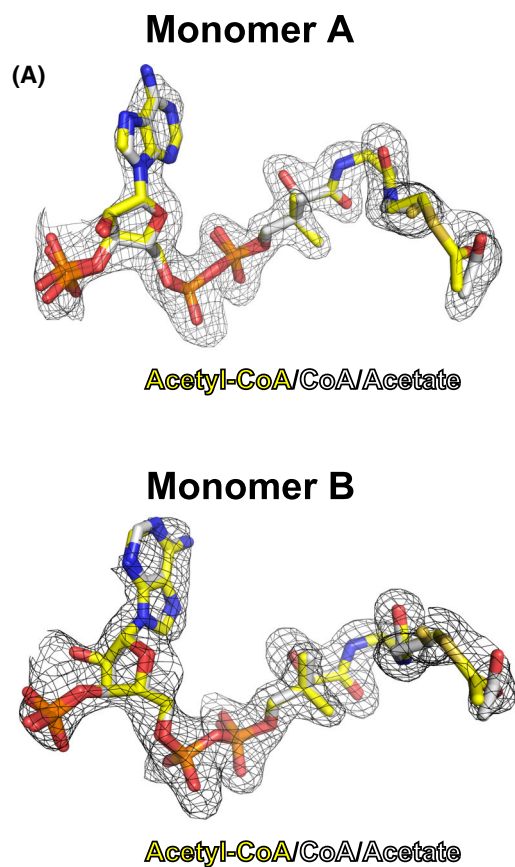
key component in protection against oxidative stress. Mycothiol is made of an acetylated Cys residue, a glucosamine residue, and an inositol group. GlmA ensures the transfer of an acetyl group from ACO to the amino group of glucosamine [50] and seems to be involved in cell wall recycling. These three enzymes have in common the ability to bind ACO and indeed residues involved in ACO binding are well conserved in the three proteins (Fig. 4). In the MshD structure, glucosamine is tightly bound by V34, E36, Q37, E79, E179, Q180, E234, Y282, and D305 [48]. In GlmA W193, E196, D287, W288, and E290 are key residues for carbohydrate binding [49]. Only a few of the residues involved in carbohydrate binding in these two enzymes are, however, conserved in MAB\_4324c, suggesting a different function for the latter (Fig. 4).

The fact that MAB\_4324c could be the mycothiol synthase in Mab cannot be excluded. A BLAST search using MshD (Rv0819) retrieves MAB\_0745 as the closest homologue of the mycothiol synthase, sharing 51% sequence identity and 61% similarity. A strong experimental argument for excluding MAB\_4324c as the main mycothiol synthase relies on the fact that, while the mycothiol synthase is an essential enzyme in mycobacteria, we were able to generate a MAB\_4324c deletion mutant in Mab, as shown below (Fig. 5). While this suggests that MAB\_4324c is unlikely to be a mycothiol synthase, we cannot rule out a redundant or closely related function that is not essential for Mab.

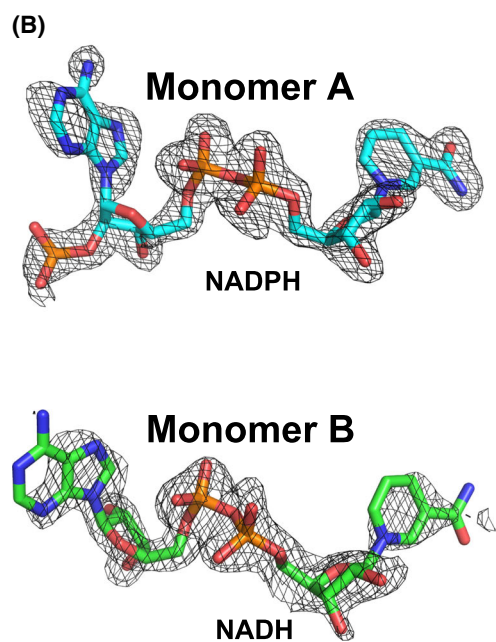
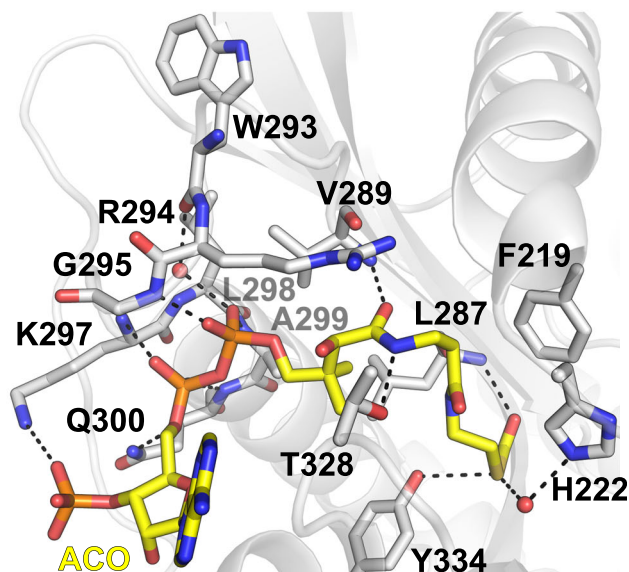
Nevertheless, the structural analysis attesting strong structural proximity with proteins involved in carbohydrate metabolism/synthetic pathway underlines the possibility that MAB\_4324c may participate in the acetylation of substrates possessing a carbohydrate moiety, which remains to be discovered.

### Closely related MAB\_4324c homologues are mainly found in actinobacteria

We searched for the presence of MAB\_4324c orthologues in other mycobacterial species, but none of them were identified in *Mycobacterium leprae*, *Mycobacterium smegmatis*, *M. tuberculosis*, or *Mycobacterium marinum*. However, additional searches using the HMMER server identified very closely related homologues in numerous bacteria, mainly within the actinobacteria phylum. Multiple sequence alignments of the best hits highlight a high conservation level with MAB\_4324c (Fig. S5). Highly conserved protein sequences were found within the *M. abscessus* complex including subspecies *M. bolletii*, and *M. massiliense* and one orthologue was found in



### Acetyl-CoA interaction as seen in Monomer A



### NADPH interaction as seen in Monomer A

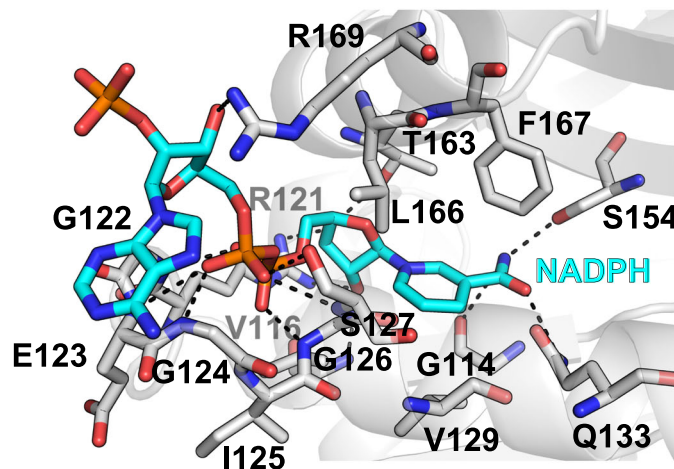


**Fig. 3.** Acetyl-CoA and NADH/NADPH recognition by MAB\_4324c. (A) Recognition of acetyl-CoA. The simulated-annealed omit maps contoured at the 3 sigma level are displayed for acetyl-CoA/CoA/acetate as seen in chains A and B. The acetyl-CoA (yellow sticks) and CoA/acetate group (white stick) were refined to an occupancy of about 0.5 each (left panels). On the right panel are displayed the interactions between the cofactor and the MAB\_4324c active site residues as seen in chain A. Hydrogen bonds are represented by the dashed lines, and water molecules are seen as red spheres. Nitrogen, oxygen, and phosphate atoms are in blue, red, and orange, respectively, while carbon atoms are in gray for MAB\_4324c amino acids or yellow for acetyl-CoA. (B) Recognition of NADH/NADPH. The simulated-annealed omit maps contoured at the 3 sigma level are displayed for NADH/NADPH as seen in chains A and B (left panels). The right panel shows the interactions occurring between NADPH and the residues side chains of MAB\_4324c as seen in chain A. The recognition of NADH is equivalent to the one of NADPH and is, therefore, not displayed.

the phylogenetically related *Mycobacterium chelonae*. Other occurrences were found in other mycobacteria, such as *Mycobacterium immunogenum* or *Mycobacterium wolinskyi* and other actinobacteria of the Streptomycetaceae, Microbacteriaceae groups as well as in a few Proteobacteria from the Burkholderiales group. This analysis indicates that the protein is not conserved necessarily in pathogenic bacteria but rather in environmental bacteria.

### **MAB\_4324c is dispensable for *M. abscessus* planktonic growth**

To investigate the role of *MAB\_4324c*, a deletion mutant was generated by the use of a homologous recombination technique enabling the production of unmarked deletion mutants in Mab (Fig. 5A) [9]. Gene deletion was obtained in the Mab smooth background. The gene deletion was confirmed by PCR genotyping and sequencing (Fig. 5B). Complementation of the deletion strain was obtained by cloning *MAB\_4324c* into the episomal pMV261 [51] yielding pMV261::*MAB\_4324c*. The same construct was used for overexpressing the protein in the WT background. A Strep-tag coding sequence was added in the 5'-end of the gene to monitor the protein expression by Western blotting. MAB\_4324c expression was indeed detected in both WT and mutant strains (Fig. 5C). All strains grew similarly to the WT progenitor, suggesting that the inactivation of MAB\_4324c does not affect the planktonic growth of Mab (Fig. 5C). The results indicate that *MAB\_4324c* is dispensable for Mab growth in planktonic culture.

### **MAB\_4324c does not trigger resistance to clinically relevant drugs**

Transcriptomic data attested that *MAB\_4324c* expression is controlled by the transcriptional WhiB7 regulator [15]. Upon stress responses, WhiB7 upregulates the expression of numerous genes and particularly

those involved in antibiotic resistance. It was notably shown that the expression of the *N*-acetyltransferase Eis2<sub>Mab</sub> that inactivates amikacin [13] is indeed controlled by WhiB7 [15]. Further, RNAseq analysis revealed that *MAB\_4324c* among other genes is upregulated upon exposure of Mab to several classes of antibiotics. *MAB\_4324c* is upregulated upon exposure to clinically relevant antibiotics such as amikacin, clarithromycin, and tigecycline [24]. We, thus, tested whether *MAB\_4324c* contributes to antibiotic resistance in Mab. To do so, MICs of a limited set of antibiotics were determined in  $\Delta$ *MAB\_4324c* and compared with those of the WT strain. However, no major differences were noticed in the drug susceptibility profile between the two strains (Table S2). Albeit, while we only tested a limited number of antibiotics, this study suggests that, in contrast to Eis2<sub>Mab</sub>, MAB\_4324c is unlikely to play a role in drug resistance mechanisms in Mab.

### **MAB\_4324c is not involved in protein acetylation**

Lysine acetylation is a ubiquitous posttranslational modification in bacteria [44], and this is particularly true in mycobacteria. In *M. tuberculosis*, about 140 proteins involved in numerous metabolic processes were shown to be acetylated [52]. We, thus, addressed the possibility that MAB\_4324c participates in protein acetylation. We compared the acetylome of the WT,  $\Delta$ *MAB\_4324c* and the corresponding MAB\_4324c-overexpressing strains by Western blotting using a pan anti-acetylated lysine primary antibody. No major differences were observed when comparing the acetylome of the four strains, suggesting that MAB\_4324c cannot acetylate proteins (Fig. S7). However, more sensitive assays, such as acetylated peptide enrichment coupled to mass spectrometry, are required to support this hypothesis. Additionally, it would be relevant to explore whether MAB\_4324c acetylates host proteins, although this is very unlikely given the fact that MAB\_4324c is not predicted to be secreted.



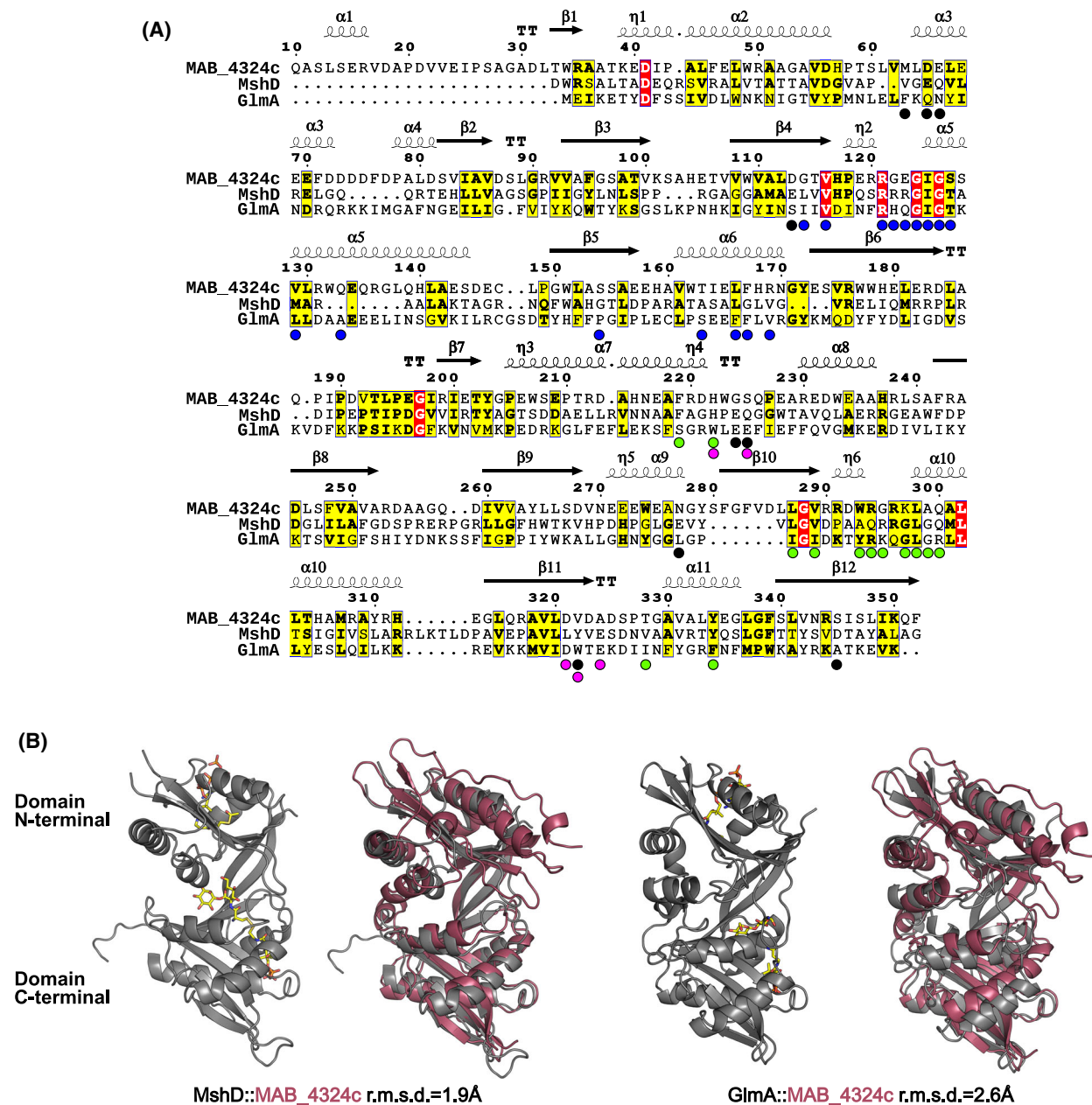


**Fig. 4.** Comparison of MAB\_4324c with structural homologues. (A) Multiple sequence alignment was performed with the ENDscript server [55] and adjusted manually with the INKScape software. The secondary structure ( $\alpha$ ,  $\alpha$ -helix,  $\beta$ ,  $\beta$ -strand,  $\eta$ ,  $3_{10}$ -helix) of MAB\_4324c obtained from its crystal structure is indicated above the alignment. Residues involved in NADPH and ACO binding in MAB\_4324c are indicated by the blue and green circles, respectively. The pink and black circles indicate the amino acids involved in carbohydrate binding in the Glucosamine/Glucosaminide *N*-acetyltransferase, GlmA (PDB id: 5KGP) and the mycothiol synthase MshD (PDB id: 2C27) crystal structures. (B) Superposition of the MshD and GlmA (both as a grey cartoon) onto the MAB\_4324c (raspberry cartoon) crystal structure. The substrates bound to MshD and GlmA are shown as yellow sticks. The r.m.s.d. values are reported below each structural alignment.

### MAB\_4324c overexpression confers intracellular survival in human macrophages

A recent RNAseq study identified a set of genes that are specifically upregulated during the intramacrophage growth of *M. massiliense* [19].

*MYCMA\_RS02565*, which is the orthologue of *MAB\_4324c* in *M. massiliense*, was four times more expressed under the intracellular conditions as compared to *in vitro* growth conditions. This prompted us to assess whether *MAB\_4324c* plays a role in the



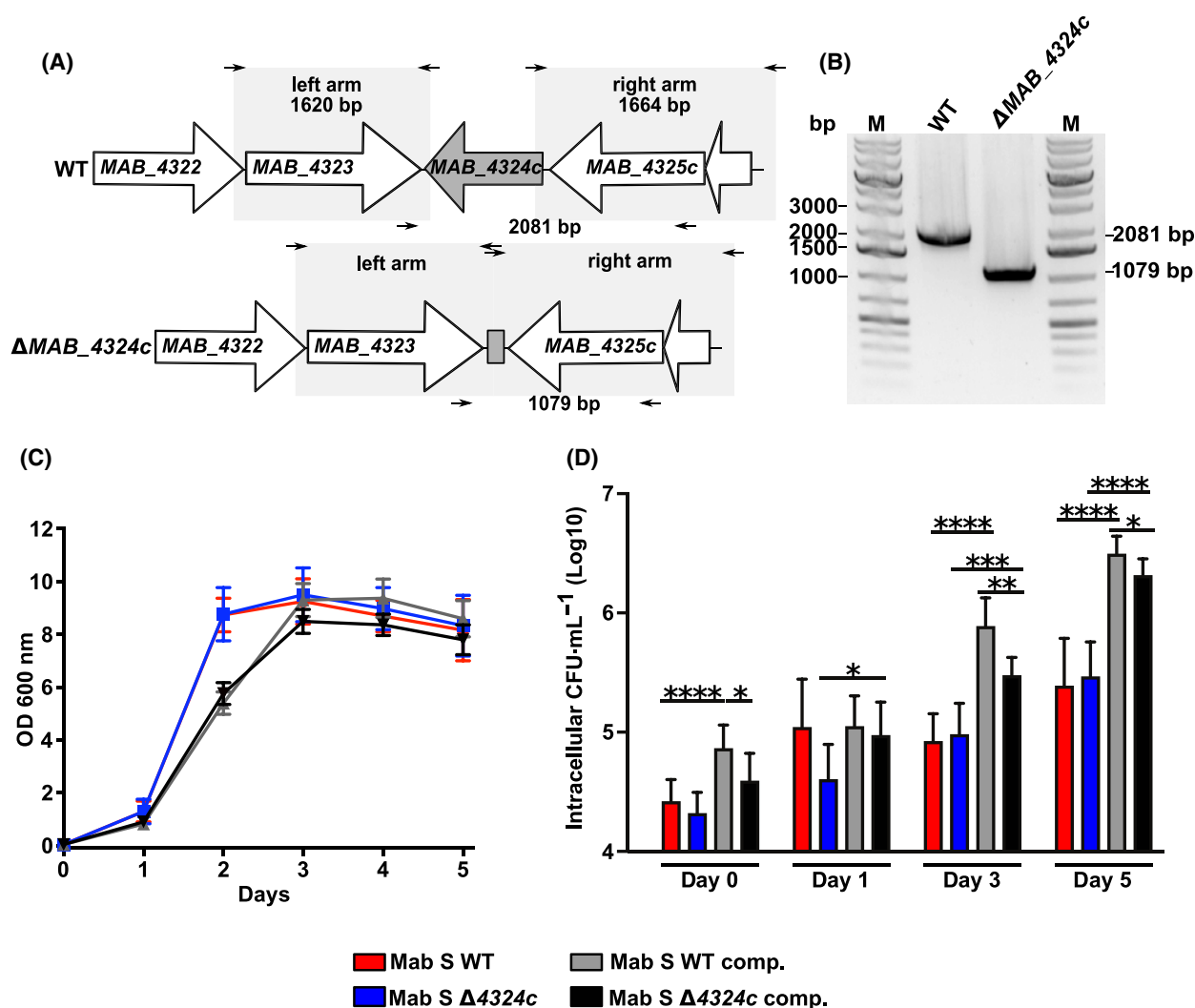


**Fig. 5.** Generation and phenotypic analyses of  $\Delta MAB_4324c$ . (A) Genomic region of *MAB\_4324c* in the parental (WT) and deletion ( $\Delta MAB_4324c$ ) strains is indicated. The size of the PCR amplicons used to genotype the  $\Delta MAB_4324c$  mutant is represented. (B) PCR genotyping demonstrates the proper deletion of the mutant strain. The PCR product of 1079 pb was amplified from  $\Delta MAB_4324c$  genomic DNA while a band at 2081 pb was obtained for the WT strain. (C) *In vitro* growth curves in liquid culture and at 37 °C of the WT smooth (Mab S WT),  $\Delta MAB_4324c$  (Mab S  $\Delta 4324c$ ), complemented strains (Mab S  $\Delta 4324c$  comp.) as well as the WT strain overexpressing *MAB\_4324c* (Mab S WT comp.). Experiments were performed in triplicates. (D) Infection of THP-1 macrophages with Mab. Histograms and error bars represent the means and standard deviations calculated from three independent experiments. For statistical analysis, the unpaired *t*-test with Welch's correction was applied. \*, \*\*, \*\*\*, and \*\*\*\* stands for  $P < 0.05$ ,  $P < 0.005$ ,  $P < 0.001$ , and  $P < 0.0001$ , respectively.

intracellular uptake and/or survival in macrophages. On day 0, the uptake of  $\Delta MAB_4324c$  was not affected as compared to the WT strain; however, the *MAB\_4324c* overexpressing strain showed increased internalization by macrophages, as determined by the CFU counts (Fig. 5D). Similarly, while  $\Delta MAB_4324c$  failed to show alterations in intracellular survival as compared to the WT strains, infections with either the complemented strain or the WT strain overproducing *MAB\_4324c* were associated with higher bacterial

loads (Fig. 5D). This suggests that overexpression of *MAB\_4324c* provides an intracellular growth advantage with an enhanced intracellular survival capacity.

While we established that *MAB\_4324c* is an active *N*-acetyltransferase, the lack of data regarding its genuine substrate makes it difficult to propose a clear function. Nonetheless, the capacity of *MAB\_4324c* to bind NADH/NADPH might explain the phenotype observed when overexpressing *MAB\_4324c* in Mab during macrophage infection. Supporting this

hypothesis, several bacterial pathogens have developed strategies to reduce the intracellular pool of  $\text{NAD}^+$ , subsequently reducing the capacity of the cell to fight against the pathogen and, therefore, thus favoring escape and intracellular survival of the bacteria [53]. Of particular interest, it has been shown that Sirtuin 3, a mitochondrial deacetylase, whose function is dependent on the  $\text{NAD}^+$  pool, enhances host defense against Mab infection [54]. Thus, by sequestering nicotinamide and diminishing the concentration of  $\text{NAD}^+$  inside the host cell, MAB\_4324c may reduce the host defense and facilitate the persistence of Mab inside macrophages. Another hypothesis somewhat related to the above one would be that MAB\_4324c by binding NADH/NADPH controls the metabolic state of this important cofactor which might be needed to convert its planktonic to an intracellular lifestyle. However, a clear demonstration of these different proposed hypotheses awaits further experimentation.

## Acknowledgements

We thank the staff at SLS beamlines for support during data collection. Funding for this work was supported by the Fondation pour la Recherche Médicale (FRM) [grant number DEQ20150331719 to LK] and the Lundbeck Foundation, Denmark (R303-2018-2964 to HA). KLU Ph.D. fellowship was supported by the National Research Agency [ANR-17-CE11-0008-01—MyTraM to MB]. MDJ received a postdoctoral fellowship granted by Labex EpiGenMed, an “Investissements d’Avenir” program (ANR-10-LABX-12-01). We would like to thank Dr W. Daher for his help with macrophage preparations. We thank Dr J. Wong for the critical reading of the manuscript.

## Author contributions

HA, KLU, JD, and MB performed experiments. MB designed research. VO performed sulfur-SAD phasing. MDJ assisted with macrophage experiments. LK and MB supervised the research. MB wrote the first draft with the input of all the authors.

## Data accessibility

The data that support the findings of this study are available from the corresponding author mickael.blaise@irim.cnrs.fr upon reasonable request. The structural data that support these findings are openly available in the wwPDB at <https://doi.org/10.2210/pdb7Q3A/pdb>.

## References

- Johansen MD, Herrmann JL, Kremer L. Non-tuberculous mycobacteria and the rise of *Mycobacterium abscessus*. *Nat Rev Microbiol*. 2020;**18**:392–407. <https://doi.org/10.1038/s41579-020-0331-1>
- Bryant JM, Grogono DM, Rodriguez-Rincon D, Everall I, Brown KP, Moreno P, et al. Emergence and spread of a human-transmissible multidrug-resistant nontuberculous mycobacterium. *Science*. 2016;**354**:751–7. <https://doi.org/10.1126/science.aaf8156>
- Bryant JM, Brown KP, Burbard S, Everall I, Belardinelli JM, Rodriguez-Rincon D, et al. Stepwise pathogenic evolution of *Mycobacterium abscessus*. *Science*. 2021;**372**:eabb8699. <https://doi.org/10.1126/science.abb8699>
- Ruis C, Bryant JM, Bell SC, Thomson R, Davidson RM, Hasan NA, et al. Dissemination of *Mycobacterium abscessus* via global transmission networks. *Nat Microbiol*. 2021;**6**:1279–88. <https://doi.org/10.1038/s41564-021-00963-3>
- Lee MR, Sheng WH, Hung CC, Yu CJ, Lee LN, Hsueh PR. *Mycobacterium abscessus* complex infections in humans. *Emerg Infect Dis*. 2015;**21**:1638–46. <https://doi.org/10.3201/2109.141634>
- Floto RA, Olivier KN, Saiman L, et al. US Cystic Fibrosis Foundation and European Cystic Fibrosis Society consensus recommendations for the management of non-tuberculous mycobacteria in individuals with cystic fibrosis. *Thorax*. 2016;**71**(Suppl 1):i1–i22. <https://doi.org/10.1136/thoraxjnl-2015-207360>
- Luthra S, Rominski A, Sander P. The role of antibiotic-target-modifying and antibiotic-modifying enzymes in *Mycobacterium abscessus* drug resistance. *Front Microbiol*. 2018;**9**:2179. <https://doi.org/10.3389/fmicb.2018.02179>
- Richard M, Gutiérrez AV, Viljoen AJ, Ghigo E, Blaise M, Kremer L. Mechanistic and structural insights into the unique TetR-dependent regulation of a drug efflux pump in *Mycobacterium abscessus*. *Front Microbiol*. 2018;**9**:649. <https://doi.org/10.3389/fmicb.2018.00649>
- Richard M, Gutiérrez AV, Viljoen A, Rodriguez-Rincon D, Roquet-Baneres F, Blaise M, et al. Mutations in the MAB\_2299c TetR regulator confer cross-resistance to clofazimine and bedaquiline in *Mycobacterium abscessus*. *Antimicrob Agents Chemother*. 2018;**63**:e01316–18. <https://doi.org/10.1128/AAC.01316-18>
- Dubée V, Bernut A, Cortes M, Lesne T, Dorcène D, Lefebvre AL, et al.  $\beta$ -Lactamase inhibition by avibactam in *Mycobacterium abscessus*. *J Antimicrob Chemother*. 2015;**70**:1051–8. <https://doi.org/10.1093/jac/dku510>

- 11 Dal Molin MD, Gut M, Rominski A, Haldimann K, Becker K, Sander P. Molecular mechanisms of intrinsic streptomycin resistance in *Mycobacterium abscessus*. *Antimicrob Agents Chemother*. 2018;**62**:e01427-17. <https://doi.org/10.1128/AAC.01427-17>
- 12 Rominski A, Selchow P, Becker K, Brülle JK, Dal Molin M, Sander P. Elucidation of *Mycobacterium abscessus* aminoglycoside and capreomycin resistance by targeted deletion of three putative resistance genes. *J Antimicrob Chemother*. 2017;**72**:2191–200. <https://doi.org/10.1093/jac/dkx125>
- 13 Ung KL, Alsarraf HMAB, Olieric V, Kremer L, Blaise M. Crystal structure of the aminoglycosides N-acetyltransferase Eis2 from *Mycobacterium abscessus*. *FEBS J*. 2019;**286**:4342–55. <https://doi.org/10.1111/febs.14975>
- 14 Ung KL, Kremer L, Blaise M. Structural analysis of the N-acetyltransferase Eis1 from *Mycobacterium abscessus* reveals the molecular determinants of its incapacity to modify aminoglycosides. *Proteins*. 2021;**89**:94–106. <https://doi.org/10.1002/prot.25997>
- 15 Hurst-Hess K, Rudra P, Ghosh P. *Mycobacterium abscessus* WhiB7 regulates a species-specific repertoire of genes to confer extreme antibiotic resistance. *Antimicrob Agents Chemother*. 2017;**61**:e01347-17. <https://doi.org/10.1128/AAC.01347-17>
- 16 Nash KA, Brown-Elliott BA, Wallace RJ Jr. A novel gene, erm(41), confers inducible macrolide resistance to clinical isolates of *Mycobacterium abscessus* but is absent from *Mycobacterium chelonae*. *Antimicrob Agents Chemother*. 2009;**53**:1367–76. <https://doi.org/10.1128/AAC.01275-08>
- 17 Richard M, Gutiérrez AV, Kremer L. Dissecting erm(41)-mediated macrolide-inducible resistance in *Mycobacterium abscessus*. *Antimicrob Agents Chemother*. 2020;**64**:e01879-19. <https://doi.org/10.1128/AAC.01879-19>
- 18 Ripoll F, Pasek S, Schenowitz C, Dossat C, Barbe V, Rottman M, et al. Non mycobacterial virulence genes in the genome of the emerging pathogen *Mycobacterium abscessus*. *PLoS One*. 2009;**4**:e5660. <https://doi.org/10.1371/journal.pone.0005660>
- 19 Dubois V, Pawlik A, Bories A, Le Moigne V, Sismeiro O, Legendre R, et al. *Mycobacterium abscessus* virulence traits unraveled by transcriptomic profiling in amoeba and macrophages. *PLoS Pathog*. 2019;**15**: e1008069. <https://doi.org/10.1371/journal.ppat.1008069>
- 20 Wei J, Dahl JL, Moulder JW, Roberts EA, O'Gaora P, Young DB, et al. Identification of a *Mycobacterium tuberculosis* gene that enhances mycobacterial survival in macrophages. *J Bacteriol*. 2000;**182**:377–84.
- 21 Duan L, Yi M, Chen J, Li S, Chen W. *Mycobacterium tuberculosis* EIS gene inhibits macrophage autophagy through up-regulation of IL-10 by increasing the acetylation of histone H3. *Biochem Biophys Res Commun*. 2016;**473**:1229–34. <https://doi.org/10.1016/j.bbrc.2016.04.045>
- 22 Green KD, Biswas T, Chang C, Wu R, Chen W, Janes BK, et al. Biochemical and structural analysis of an Eis family aminoglycoside acetyltransferase from *Bacillus anthracis*. *Biochemistry*. 2015;**54**:3197–206. <https://doi.org/10.1021/acs.biochem.5b00244>
- 23 Chen W, Biswas T, Porter VR, Tsodikov OV, Garneau-Tsodikova S. Unusual regioversatility of acetyltransferase Eis, a cause of drug resistance in XDR-TB. *Proc Natl Acad Sci USA*. 2011;**108**:9804–8. <https://doi.org/10.1073/pnas.1105379108>
- 24 Schildkraut JA, Coolen JPM, Burbard S, Sangen JJN, Kwint MP, Floto RA, et al. RNA-sequencing elucidates drug-specific mechanisms of antibiotic tolerance and resistance in *M. abscessus*. *Antimicrob Agents Chemother*. 2021;**66**:e0150921. <https://doi.org/10.1128/AAC.01509-21>
- 25 Henrich B, Bergamaschi A, Broennimann C, Dinapoli R, Eikenberry EF, Johnson I, et al. PILATUS: a single photon counting pixel detector for X-ray applications. *Nucl Instrum Methods Phys Res A*. 2009;**607**:247–9. <https://doi.org/10.1016/j.nima.2009.03.200>
- 26 Waltersperger S, Olieric V, Pradervand C, Gletting W, Salathe M, Fuchs MR, et al. PRiGo: a new multi-axis goniometer for macromolecular crystallography. *J Synchrotron Radiat*. 2015;**22**:895–900. <https://doi.org/10.1107/S1600577515005354>
- 27 Weinert T, Olieric V, Waltersperger S, Panepucci E, Chen L, Zhang H, et al. Fast native-SAD phasing for routine macromolecular structure determination. *Nat Methods*. 2015;**12**:131–3. <https://doi.org/10.1038/nmeth.3211>
- 28 Kabsch W. Integration, scaling, space-group assignment and post-refinement. *Acta Crystallogr D Biol Crystallogr*. 2010;**66**(Pt 2):133–44. <https://doi.org/10.1107/S0907444909047374>
- 29 Karplus PA, Diederichs K. Linking crystallographic model and data quality. *Science*. 2012;**336**:1030–3. <https://doi.org/10.1126/science.1218231>
- 30 Sheldrick GM. A short history of SHELX. *Acta Crystallogr A*. 2008;**64**:112–22. <https://doi.org/10.1107/S0108767307043930>
- 31 Usón I, Sheldrick GM. An introduction to experimental phasing of macromolecules illustrated by SHELX; new autotracing features. *Acta Crystallogr Sect Struct Biol*. 2018;**74**:106–16. <https://doi.org/10.1107/S2059798317015121>
- 32 Skubák P, Pannu NS. Automatic protein structure solution from weak X-ray data. *Nat Commun*. 2013;**4**:2777. <https://doi.org/10.1038/ncomms3777>
- 33 Emsley P, Lohkamp B, Scott WG, Cowtan K. Features and development of Coot. *Acta Crystallogr D Biol Crystallogr*. 2010;**66**(Pt 4):486–501. <https://doi.org/10.1107/S0907444910007493>

- 34 Adams PD, Afonine PV, Bunkóczi G, et al. PHENIX: a comprehensive Python-based system for macromolecular structure solution. *Acta Crystallogr D Biol Crystallogr*. 2010;**66**:213–21. <https://doi.org/10.1107/S0907444909052925>
- 35 Richard M, Gutiérrez AV, Viljoen A, Rodriguez-Rincon D, Roquet-Baneres F, Blaise M, et al. Mutations in the MAB\_2299c TetR regulator confer cross-resistance to clofazimine and bedaquiline in *Mycobacterium abscessus*. *Antimicrob Agents Chemother*. 2019;**63**:e01316–18. <https://doi.org/10.1128/AAC.01316-18>
- 36 Stover CK, de la Cruz VF, Fuerst TR, et al. New use of BCG for recombinant vaccines. *Nature*. 1991;**351**:456–60. <https://doi.org/10.1038/351456a0>
- 37 Woods GL, Brown-Elliott BA, Conville PS, Desmond EP, Hall GS, Lin G, et al. Susceptibility testing of mycobacteria, nocardiae, and other aerobic actinomycetes. 2nd ed. Wayne, PA: Clinical and Laboratory Standards Institute; 2011 [cited 2020 Oct 22]. Available from: <http://www.ncbi.nlm.nih.gov/books/NBK544374/>
- 38 Mistry J, Chuguransky S, Williams L, Qureshi M, Salazar GA, Sonnhammer ELL, et al. Pfam: the protein families database in 2021. *Nucleic Acids Res*. 2021;**49**(D1):D412–9. <https://doi.org/10.1093/nar/gkaa913>
- 39 Kuhn ML, Majorek KA, Minor W, Anderson WF. Broad-substrate screen as a tool to identify substrates for bacterial Gcn5-related N-acetyltransferases with unknown substrate specificity. *Protein Sci*. 2013;**22**:222–30. <https://doi.org/10.1002/pro.2199>
- 40 Pan Q, Zhao F-L, Ye B-C. Eis, a novel family of arylalkylamine N-acetyltransferase (EC 2.3.1.87). *Sci Rep*. 2018;**8**:1–8. <https://doi.org/10.1038/s41598-018-20802-6>
- 41 Hodel A, Kim SH, Brünger AT. Model bias in macromolecular crystal structures. *Acta Crystallogr A*. 1992;**48**:851–8. <https://doi.org/10.1107/S0108767392006044>
- 42 Vetting MW, Bareich DC, Yu M, Blanchard JS. Crystal structure of RimI from *Salmonella typhimurium* LT2, the GNAT responsible for N $\alpha$ -acetylation of ribosomal protein S18. *Protein Sci*. 2008;**17**:1781–90. <https://doi.org/10.1110/ps.035899.108>
- 43 Christensen DG, Meyer JG, Baumgartner JT, et al. Identification of novel protein lysine acetyltransferases in *Escherichia coli*. *MBio*. 2018;**9**:e01905–18. <https://doi.org/10.1128/mBio.01905-18>
- 44 Lammers M. Post-translational lysine ac(ety)lation in bacteria: a biochemical, structural, and synthetic biological perspective. *Front Microbiol*. 2021;**12**:757179. <https://doi.org/10.3389/fmicb.2021.757179>
- 45 Nambi S, Basu N, Visweswariah SS. cAMP-regulated protein lysine acetylases in mycobacteria. *J Biol Chem*. 2010;**285**:24313–23. <https://doi.org/10.1074/jbc.M110.118398>
- 46 Lee HJ, Lang PT, Fortune SM, Sasseti CM, Alber T. Cyclic-AMP regulation of protein lysine acetylation in *Mycobacterium tuberculosis*. *Nat Struct Mol Biol*. 2012;**19**:811–8. <https://doi.org/10.1038/nsmb.2318>
- 47 Liu XX, Liu WB, Ye BC. Regulation of a protein acetyltransferase in *Myxococcus xanthus* by the coenzyme NADP. *J Bacteriol*. 2015;**198**:623–32. <https://doi.org/10.1128/JB.00661-15>
- 48 Vetting MW, Yu M, Rendle PM, Blanchard JS. The substrate-induced conformational change of *Mycobacterium tuberculosis* mycothiol synthase. *J Biol Chem*. 2006;**281**:2795–802. <https://doi.org/10.1074/jbc.M510798200>
- 49 Dopkins BJ, Tipton PA, Thoden JB, Holden HM. Structural studies on a glucosamine/glucosaminide N-acetyltransferase. *Biochemistry*. 2016;**55**:4495–508. <https://doi.org/10.1021/acs.biochem.6b00536>
- 50 Reith J, Mayer C. Characterization of a glucosamine/glucosaminide N-acetyltransferase of *Clostridium acetobutylicum*. *J Bacteriol*. 2011;**193**:5393–9. <https://doi.org/10.1128/JB.05519-11>
- 51 Stover CK, de la Cruz VF, Fuerst TR, Burlein JE, Benson LA, Bennett LT, et al. New use of BCG for recombinant vaccines. *Nature*. 1991;**351**:456–60. <https://doi.org/10.1038/351456a0>
- 52 Liu F, Yang M, Wang X, Yang S, Gu J, Zhou J, et al. Acetylome analysis reveals diverse functions of lysine acetylation in *Mycobacterium tuberculosis*. *Mol Cell Proteomics*. 2014;**13**:3352–66. <https://doi.org/10.1074/mcp.M114.041962>
- 53 Roussin M, Salcedo SP. NAD<sup>+</sup>-targeting by bacteria: an emerging weapon in pathogenesis. *FEMS Microbiol Rev*. 2021;**45**:fuab037. <https://doi.org/10.1093/femsre/fuab037>
- 54 Kim YJ, Lee SH, Jeon SM, Silwal P, Seo JY, Hanh BTB, et al. Sirtuin 3 is essential for host defense against *Mycobacterium abscessus* infection through regulation of mitochondrial homeostasis. *Virulence*. 2020;**11**:1225–39. <https://doi.org/10.1080/21505594.2020.1809961>
- 55 Robert X, Gouet P. Deciphering key features in protein structures with the new ENDscript server. *Nucleic Acids Res*. 2014;**42**(Web Server issue):W320–4. <https://doi.org/10.1093/nar/gku316>

## Supporting information

Additional supporting information may be found online in the Supporting Information section at the end of the article.

**Fig. S1.** Measurement of the MAB\_4324c dependent N-acetyltransferase activity.

**Fig. S2.** Modelling and refinement of the ligands.

**Fig. S3.** UV spectrum of pure MAB\_4324c expressed in *E. coli*.



**Fig. S4.** NADH or NADPH do not modulate MAB\_4324c enzymatic activity.

**Fig. S5.** Multiple sequence alignments of the MAB\_4324c orthologues.

**Fig. S6.** Western blot confirming the expression of MAB\_4324c.

**Fig. S7.** *M. abscessus* acetylome revealed by an anti-acetyl lysine antibody.

**Table S1.** Kinetic parameters of MAB\_4324c in presence of NADH and NADPH.

**Table S2.** Determination of the MIC<sub>99</sub>.